Appl. Phys. B 89, 367–376 (2007)
DOI: 10.1007/s00340-007-2808-2

Applied Physics B
Lasers and Optics

JUN DONG[1,✉]
A. SHIRAKAWA[1]
K.-I. UEDA[1]
A.A. KAMINSKII[2]

Effect of ytterbium concentration on cw Yb:YAG microchip laser performance at ambient temperature – Part II: Theoretical modeling

[1] Institute for Laser Science, University of Electro-Communications, 1-5-1 Chofugaoka, Chofu, Tokyo 182-8585, Japan
[2] Crystal Laser Physics Laboratory, Institute of Crystallography, Russian Academy of Sciences, Leninsky Pr. 59, Moscow 119333, Russia

Received: 11 September 2007 /
Revised version: 16 September 2007
Published online: 21 October 2007 •

ABSTRACT A theoretical model based on a quasi-four-level system is modified to investigate the effect of Yb concentration on performance of continuous-wave Yb:YAG microchip lasers by taking into account temperature-dependent thermal population distribution, temperature-dependent emission cross-section and concentration-dependent fluorescence lifetime, thermal loading, thermal conductivity, and thermal expansion coefficient. The local temperature rise in Yb:YAG crystal caused by the absorbed pump power plays an important role in the laser performance of Yb:YAG microchip lasers working at ambient temperature without actively cooling the sample. The output wavelengths dependent on output coupling, Yb concentration, and pump power level were analyzed quantitatively. The numerical simulation of Yb:YAG microchip lasers is in good agreement with experimental data. The optimized laser operation for Yb:YAG microchip lasers is proposed by varying the thickness and output coupling for different Yb concentrations. The effect of thermal lens, thermal deformation effect, and saturated inversion population distribution inside the Yb:YAG crystal on performance of heavy-doped Yb:YAG microchip lasers are also addressed.

PACS 42.55.Xi; 42.70.Hj; 42.55.Rz

1 Introduction

With the rapid development of high power, high brightness InGaAs laser diodes emitting at 940 nm, much effort has been exerted to develop high power, laser-diode-pumped, ytterbium-doped solid-state lasers. Among ytterbium-doped solid-state laser materials, Yb:YAG has been a promising candidate for high-power laser-diode (LD)-pumped solid-state lasers [1, 2], because YAG is an attractive host material with excellent thermal, chemical and mechanical properties [3]. Yb:YAG crystals have several advantages, such as a long storage lifetime (about 1 ms) [4, 5], a very low quantum defect resulting in three times less heat generation during lasing than comparable Nd-doped laser systems [6], a broad absorption bandwidth and less sensitivity to diode wavelength specifications [5, 7], and easy growth of high quality and moderate ytterbium contain crystals without luminescence quenching [8]. However, the quasi-four-level system of ytterbium-doped materials limits the laser performance of these materials by the thermal population of terminated lasing levels of the $^2F_{7/2}$ state (especially for 1030 nm oscillation at $\approx 612\ \mathrm{cm}^{-1}$ terminated laser level) [5], which contains $\approx 5\%$ of the $^2F_{7/2}$ population at room temperature (RT). Therefore, temperature controlling Yb:YAG crystals is an important factor in the design of high power lasers. High average output power lasers based on Yb:YAG have been achieved with high efficiency by using different laser cavity configurations such as end-pumped microchip lasers, edge-pumped, and side-pumped laser systems [9–13] to control the temperature of the working Yb:YAG part. Some of the applications require that the lasers should be compact and economic; therefore, the cooling system is eliminated for compact and easily maintainable laser system. Thus, laser-diode end-pumped microchip lasers are a better choice to achieve highly efficient laser operation under high pump power intensity. The effect becomes worse at high temperature induced by the heat generated by the absorbed pump power inside the Yb:YAG crystals. In addition, the thermal population still depends strongly on the concentration of Yb^{3+} lasants in YAG crystal. Therefore, high pump power intensity is required to realize highly efficient performance of Yb:YAG microchip lasers at room temperature without active cooling of the working Yb:YAG crystal. The effect of Yb concentration of these microchip lasers has been investigated systematically and found that the Yb concentration has great effect on laser performance, owing to the strong reabsorption loss and thermal lens effect [14].

Several theoretical models for investigation of end-pumped quasi-four-level lasers [15, 16] have been proposed by taking into account the reabsorption losses; however, previous theoretical modeling of quasi-four-level lasers focused on the 946 nm oscillation from Nd:YAG crystals and did not take into account concentration-dependent fluorescence lifetime. Recently, some theoretical models have been proposed for describing end-pumped quasi-three-level lasers, such as Tm^{3+}:YVO_4, Ti:sapphire, and Yb:YAG lasers [17–20]. Although the reabsorption loss and concentration quenching effect were included in the theoretical modeling of Yb:YAG

✉ Fax: +81-0424-85-8960, E-mail: dong@ils.uec.ac.jp

microchip lasers [19], the model is concentrated on laser performance under sufficient temperature control of the gain medium, the thermal effect induced by the absorbed pump power was not included in the model. The thermal conductivity of YAG decreases and thermal loading parameter increases with increasing ytterbium concentration. Furthermore, there is strong emission quenching, which is attributed to uncontrolled impurities during crystal growth. These concentration-dependent thermal properties of Yb:YAG have great unwanted effects on the laser performance of Yb:YAG microchip laser at ambient temperature without sufficient active cooling system. The thermal conductivity, thermal expansion coefficient, thermal loading of Yb:YAG crystals also relate to the temperature, temperature rise-induced by the pump power deposited on the gain medium are important factors to be considered in the laser performance of Yb:YAG at ambient temperature. Also temperature has great impact on the emission peak cross-section of Yb:YAG crystals [21, 22]. It is necessary to establish a theoretical model to include all above-mentioned thermal properties of Yb:YAG crystals.

In this paper, we report on the theoretical investigation of the effect of Yb^{3+}-ion concentration on the development of Yb:YAG microchip lasers at ambient temperature. The operating characteristics of Yb:YAG microchip lasers were investigated based on the well-established rate equations [15, 16] by taking into account the temperature-dependent reabsorption loss of quasi-four-level system and temperature effects due to the heat generated by the absorbed pump power. The numerical simulation results are in very good agreement with the experimental data presented in Part I of this paper [14]. Although there is strong reabsorption loss for Yb:YAG microchip lasers working at room temperature without sufficient cooling the samples, the performance of such microchip lasers can be further improved by choosing optimized thickness and output coupling. Comparable laser performance can be achieved in certain working condition by using heavy-doped Yb:YAG crystals. The theoretical modeling of such microchip lasers shows that better laser performance can be achieved by using Yb:YAG crystal doped with lower ytterbium concentration. The laser properties at 1030 nm become worse than those at 1049 nm with the Yb^{3+}-ion concentration owing to the strong thermal population distribution in its pump area. The effect of thermal lens and saturated inversion population distribution inside the gain medium on the performance of Yb:YAG microchip lasers are also addressed for different Yb concentrations and output coupling under different pump power levels.

2 Theoretical analysis of Yb:YAG microchip lasers

Microchip lasers are formed by directly coating the dielectric films on the surfaces of the gain medium to form the laser cavities, so in principle, they are Fabry–Pérot cavities. On the other hand, microchip lasers can be formed by directly coating the dielectric film on one surface of the gain medium to form the rear mirror of the laser cavity; the output coupler is separated from the gain medium which can be easily adjusted for optimizing other parameters to achieve optimized operation of such a laser system. The cavities can be treated as approximately concave-concave types with the thermal effects of the media taken into account or plane-concave cavities. When the pump and laser beam in the gain media are assumed to be Gaussian beams, using an M^2 factor, the radii of the pump and laser beams along the direction of the light can be written as [20, 23]

$$w_{\mathrm{p}}^2(z) = w_{\mathrm{p0}}^2\left[1+\frac{(M^2)^2\lambda_{\mathrm{p}}^2(z-z_0)^2}{\pi^2 w_{\mathrm{p0}}^4 n^2}\right], \tag{1}$$

$$w_{\mathrm{L}}^2(z) = w_{\mathrm{L0}}^2\left[1+\frac{\lambda_{\mathrm{L}}^2(z-z_0)^2}{\pi^2 w_{\mathrm{L0}}^4 n^2}\right], \tag{2}$$

where z is the coordinate along the axis of the laser, $w_{\mathrm{p}}(z)$ and $w_{\mathrm{L}}(z)$ are the radii of the pump and the laser beams at z, w_{p0} and w_{L0} are the radii of the pump and the laser beams at waist $z = z_0$, λ_{p} and λ_{L} are the wavelengths of the pump and the laser, n is the refractive index of the gain media. Generally, the length of the microchip gain media is less than several millimeters; therefore, the approximation of $w_{\mathrm{p}}(z) = w_{\mathrm{p0}}$ and $w_{\mathrm{L}}(z) = w_{\mathrm{L0}}$ may be adopted.

For a laser gain medium pumped by longitudinally cw incident pump power P_0, the pump rate can be written as $W_{\mathrm{p}} = P_0\eta_{\mathrm{a}}/h\nu_{\mathrm{p}}$, where h is the Planck constant, ν_{p} is the frequency of the pump power, $\eta_{\mathrm{a}} = 1-\exp(-\alpha l)$ is the fraction of the incident pump power absorbed by a laser gain medium of thickness l for one-pass pumping configuration, and α is the absorption coefficient at pump wavelength λ_{p}. The normalized functions that describe the spatial distribution of the pump power and the spatial distribution of the laser cavity mode can be expressed as [16]

$$r_{\mathrm{p}}(r,z) = \frac{2\alpha}{\pi w_{\mathrm{p0}}^2\eta_{\mathrm{a}}}\exp\left(\frac{-2r^2}{w_{\mathrm{p0}}^2}\right)\exp(-\alpha z), \tag{3}$$

$$\phi_{\mathrm{L}}(r,z) = \frac{2}{\pi w_{\mathrm{L0}}^2 l_{\mathrm{c}}}\exp\left(\frac{-2r^2}{w_{\mathrm{L0}}^2}\right). \tag{4}$$

The total number of the laser photons in the cavity is defined as $\Phi = 2l_{\mathrm{c}}P_{\mathrm{c}}/hc\nu_{\mathrm{L}}$, where P_{c} is the laser power inside the cavity, c is the vacuum speed of the light, and ν_{L} is the frequency of the laser emission, l_{c} is the optical length of the resonator.

For the end-pumped microchip lasers, owing to the small pump beam diameter compared to the diameter of the gain medium, the heat flow prefers along the radius direction; therefore, the temperature distribution in the gain medium for end-pumped laser can be written as, according to [24],

$$T(r,z) = T_{\mathrm{c}} + \frac{P_{\mathrm{h}}(z)}{4\pi k}\left[\ln\left(\frac{R^2}{r^2}\right) + E_i\left(\frac{2R^2}{w_{\mathrm{p0}}^2}\right) - E_i\left(\frac{2r^2}{w_{\mathrm{p0}}^2}\right)\right], \tag{5}$$

where T_{c} is the coolant temperature at $r = R$, r is the transverse radial coordinate, k is the thermal conductivity of the gain medium, R is the radius of the gain medium or the aperture of the cooler, $P_{\mathrm{h}}(z)$ is the heat generated inside the gain medium when the incident pump power is P_0, $P_{\mathrm{h}}(z) = P_0\alpha\exp(-\alpha z)f_{\mathrm{h}}$, f_{h} is the thermal loading parameter of gain materials, $E_i(x)$ is the exponential integral function: $E_i(x) = \int_x^\infty\left(\frac{\mathrm{e}^{-t}}{t}\right)\mathrm{d}t$. For the end-pumped microchip lasers, the temperature variation along the z-axis is smaller than that along

the radial direction, so the average temperature along the z-axis is adopted in calculation of the thermal lens effect and numerical simulations of the laser performance. Therefore, the temperature distribution inside the gain medium can be expressed as

$$T(r) = T_c + \frac{P_h}{4\pi k l}\left[\ln\left(\frac{R^2}{r^2}\right) + E_i\left(\frac{2R^2}{w_{p0}^2}\right) - E_i\left(\frac{2r^2}{w_{p0}^2}\right)\right], \tag{6}$$

where $P_h = P_0\eta_a f_h$ is the total heat generated inside the gain medium when the incident pump power of P_0 is applied.

The thermally induced lens is so far the most bothering issue in the development of high power solid-state lasers and limits the laser output power with good beam quality to a narrow pump power range. Longitudinal pumping leads to the most pronounced nonuniform heating distribution resulting from the localized absorption of the pump radiation, this effect becomes more severe with high concentration doping in Yb:YAG crystals. For a microchip laser that is end-pumped by a fiber-coupled laser-diode, the thermal lens makes the resonator stable, and the focal length of the thermal lens, f_{th}, is given by [25, 26]

$$f_{th} = \frac{\pi w_p^2 k}{f_h P_0 \eta_a}\left[\frac{dn}{dT} + (n-1)(1+\nu)\alpha_e + n^3\alpha_e C_r\right]^{-1}, \tag{7}$$

where dn/dT is the thermal dispersion, α_e is the thermal expansion coefficient, n is the refractive index, C_r is the elasto-optical coefficient, ν is the Pisson's ratio, and w_p is the average pump beam waist in the active medium. The focus length of the thermal lens depends on the square of the pump beam radius and incident pump power.

Owing to the pronounced heat distribution in the pump section, the thermal lens can be assumed to be located at surface with high reflectivity at lasing wavelength. The *ABCD* matrix M for a round trip optical path starting from the output mirror of microchip lasers can be expressed as [27, 28]

$$M = \begin{pmatrix} 1-(2l/nf_{th}) & 2(l/n - l^2/n^2 f_{th}) \\ -2/f_{th} & 1-(2l/nf_{th}) \end{pmatrix}. \tag{8}$$

From the stable laser cavity condition, there exits a critical pump power, $P_{critical}$, at which the thermally induced lens causes the laser cavity to be unstable, the critical thermal lens that relates to the stability of microchip laser cavity is given by

$$f_{th,critical} = 2l/n\,. \tag{9}$$

Comparing (7) and (9), the critical pump power can be expressed as

$$P_{0,critical} = \frac{\pi w_p^2 k n}{2l f_h \eta_a}\left[\frac{dn}{dT} + (n-1)(1+\nu)\alpha_e + n^3\alpha_e C_r\right]^{-1}. \tag{10}$$

Thermal conductivity, thermal expansion coefficient, and thermal dispersion all have strong relationship with temperature, the commonly cited thermal conductivity of undoped YAG crystal is 0.103 W/(cm K) [29]. However, the thermal conductivity decreases with increasing of the Yb^{3+}-ion concentration in YAG crystal, such as 0.078, 0.073, and 0.055 W/(cm K) for 5, 15, and 25 at. % Yb:YAG measured in [8]. The temperature-dependent thermal conductivity of undoped YAG was described as

$$k(T) = \frac{a}{(\ln(bT))^c} - \frac{d}{T}, \tag{11}$$

where $a = 1.9\times10^{-7}$ W/(cm K), $b = 5.33$ K^{-1}, $c = 7.14$, and $d = 331$ W/cm.

The change in refractive index of YAG with temperature dn/dT can be calculated from the change in optical path length with temperature and thermal expansion coefficient α_e with temperature as follows [30, 31]:

$$\frac{dn}{dT}(T) = n(\gamma(T) - \alpha_e(T))\,. \tag{12}$$

$\gamma(T)$ is the fractional change in optical path length with temperature, which can be determined from the period of the interference fringe pattern as follows [30]:

$$\gamma(T) = \frac{1}{nL}\frac{d(nL)}{dT}\,. \tag{13}$$

The temperature dependence of $\gamma(T)$ can be fitted with the experimental data in [30] as

$$\gamma(T) = 4.49\times10^{-8}\,T - 1.56\times10^{-6}\,. \tag{14}$$

For thermal expansion coefficient, α_e, we adopt [32]

$$\alpha_e(T) = a' T^{b'}\,, \tag{15}$$

where $a' = 1.14\times10^{-6}$ K$^{-(b'+1)}$ and $b' = 0.69$.

The temperature of Yb:YAG crystal rises with pump power working at ambient temperature, the thermal conductivity is lower, and the thermal expansion coefficient and the thermal dispersion are larger. Therefore, the thermal lens effect becomes severe and the critical pump power decreases with local temperature rise inside the gain medium.

Because Yb:YAG laser at RT is a quasi-four-level system, the reabsorption of the ground state has a great effect on the laser performance, the rate equations including the luminescence concentration quenching and the reabsorption of the ground state in steady state can be described as [15, 16, 33]

$$\frac{d\Delta N(r,z)}{dt} = fW_p r_p(r,z) - \frac{\Delta N(r,z) + f_{low}N_{tot}}{\tau(N_{tot})} - \frac{fc\sigma\Delta N(r,z)}{n}\Phi\phi_L(r,z=0)\,, \tag{16}$$

where $\Delta N(r,z)$ is the spatial distribution of the population inversion density between upper and lower laser levels under pumped conditions, σ is the emission peak cross-section of the gain crystal at the laser wavelength, which depends on the temperature, f_{low} and f_{up} are the Boltzmann factors at the terminated and the upper laser levels of the Yb:YAG crystal, respectively; $f = f_{low} + f_{up}$; $\tau(N_{tot})$ is the lifetime of the upper laser level as a function of the concentration of the active ions.

Figure 1 shows the energy-level diagram of Yb:YAG crystal and energy gap of each Stark levels from the ground state.

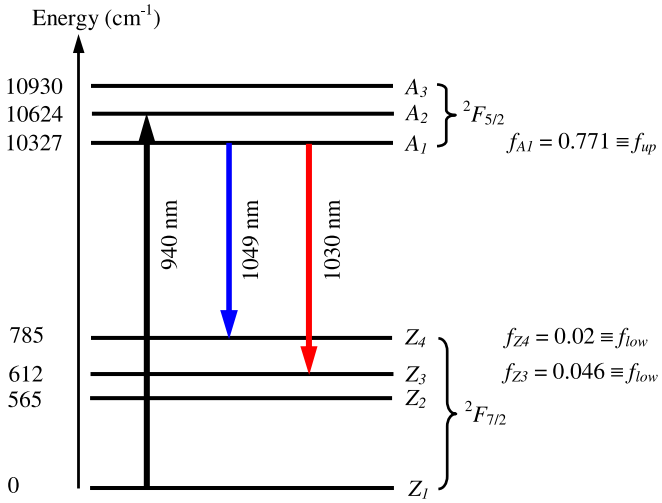

FIGURE 1 Energy level diagram of the Yb:YAG crystal. The pump and laser transitions are noted by the *heavy lines*. The calculated Boltzmann occupancies at up laser level and terminated laser levels (612 and 785 cm^{-1}) at room temperature are also shown

It is assumed that there is rapid thermalization of the levels within each manifold so that the relative populations of the sublevels within a manifold can be treated as Boltzmann distribution. The Boltzmann distribution factor at the upper laser level and the terminated laser levels (612 cm^{-1} for 1030 nm oscillation and 785 cm^{-1} for 1049 nm oscillation) of Yb:YAG crystal can be described as follows:

$$f_{\mathrm{up}} = \exp(-E_{A1}/k_{\mathrm{B}}T)/\sum_i \exp(-E_{Ai}/k_{\mathrm{B}}T)\,, \tag{17}$$

$$f_{\mathrm{low}} = \exp(-E_{Z3}/k_{\mathrm{B}}T)/\sum_i \exp(-E_{Zi}/k_{\mathrm{B}}T)\,, \tag{18}$$

where k_{B} is the Boltzmann constant and T is the temperature. f_{low} should be calculated by replacing E_{Z3} with E_{Z4} when the laser oscillates at 1049 nm. f_{up} and f_{low} are strongly dependent on the temperature of Yb:YAG, f_{low} increases with temperature, especially for 1030 nm oscillation.

The corresponding equation for the total number Φ of photons in the cavity is [15, 16]

$$\frac{\mathrm{d}\Phi}{\mathrm{d}t} = \frac{c\sigma}{n}\iiint \Delta N(r,z)\Phi\phi_{\mathrm{L}}(r,z)\,\mathrm{d}V - \frac{\Phi}{\tau_q} = 0\,, \tag{19}$$

where $\tau_q = \frac{2l_{\mathrm{c}}}{c(L+T_{\mathrm{oc}})}$ is the cold-cavity photon lifetime, L is the round-trip loss and can be expressed as $L = 2\delta l$, δ is the internal loss per unit length in the laser gain medium which has strong dependence on the Yb^{3+}-ion concentration, and l_{c} is the optical length of the resonator, T_{oc} is the output coupler transmission.

From (16), the spatial distribution of the population inversion density is given by

$$\begin{aligned}\Delta N(r,z) &= \frac{W_{\mathrm{p}}\tau(N_{\mathrm{tot}})r_{\mathrm{p}}(r,z) - f_{\mathrm{low}}N_{\mathrm{tot}}}{1+\frac{c\tau(N_{\mathrm{tot}})\sigma}{n}\Phi\phi_{\mathrm{L}}(r,z)} \\ &= \frac{\Delta N_{\mathrm{p}}(r,z) - f_{\mathrm{low}}N_{\mathrm{tot}}}{1+\frac{I_{\mathrm{L}}(r,z)}{I_{\mathrm{s}}}},\end{aligned} \tag{20}$$

where $I_{\mathrm{L}}(r,z)$ is the intracavity laser intensity, I_{s} is the saturated intensity of Yb:YAG crystal, $\Delta N_{\mathrm{p}}(r,z)$ is the pump power-induced inversion population.

Substitute the saturated inversion population density given in (20) into (19), an implicit relationship between the pump power P_0 and the total laser power P_{c} inside the cavity can be expressed as

$$\begin{aligned}&4\pi l\sigma\int_0^l\int_0^\infty \frac{\tau(N_{\mathrm{tot}})\frac{P_0\eta_{\mathrm{a}}}{h\nu_{\mathrm{p}}}r_{\mathrm{p}}(r,z) - f_{\mathrm{low}}N_{\mathrm{tot}}}{1+\frac{\tau(N_{\mathrm{tot}})\sigma}{n}\frac{2nlP_{\mathrm{c}}}{h\nu_{\mathrm{L}}}\phi_{\mathrm{L}}(r,z)}\phi_{\mathrm{L}}(r,z)r\,\mathrm{d}r\,\mathrm{d}z \\ &= L + T_{\mathrm{oc}}\,.\end{aligned} \tag{21}$$

When the spatial distributions of the pump power and laser power inside the cavity (3) and (4) are substituted into (21), (21) can be rewritten as

$$\begin{aligned}&\frac{8\sigma}{w_{\mathrm{L0}}^2}\int_0^l\int_0^\infty \frac{\tau(N_{\mathrm{tot}})\frac{2\alpha P_0}{h\nu_{\mathrm{p}}\pi w_{\mathrm{p0}}^2}\exp\left(\frac{-2r^2}{w_{\mathrm{p0}}^2}\right)\exp(-\alpha z) - f_{\mathrm{low}}N_{\mathrm{tot}}}{1+\frac{4P_{\mathrm{c}}\tau(N_{\mathrm{tot}})\sigma}{h\nu_{\mathrm{L}}\pi w_{\mathrm{L0}}^2}\exp\left(\frac{-2r^2}{w_{\mathrm{L0}}^2}\right)} \\ &\exp\left(\frac{-2r^2}{w_{\mathrm{L0}}^2}\right)r\,\mathrm{d}r\,\mathrm{d}z = L + T_{\mathrm{oc}}\,.\end{aligned} \tag{22}$$

Equation (22) can be simplified by integrating over the length of the gain medium, then

$$\begin{aligned}&\frac{8\sigma}{w_{\mathrm{L0}}^2}\int_0^\infty \frac{\tau(N_{\mathrm{tot}})\frac{2P_0}{h\nu_{\mathrm{p}}\pi w_{\mathrm{p0}}^2}\exp\left(\frac{-2r^2}{w_{\mathrm{p0}}^2}\right)\eta_{\mathrm{a}} - f_{\mathrm{low}}N_{\mathrm{tot}}l}{1+\frac{4P_{\mathrm{c}}\tau(N_{\mathrm{tot}})\sigma}{h\nu_{\mathrm{L}}\pi w_{\mathrm{L0}}^2}\exp\left(\frac{-2r^2}{w_{\mathrm{L0}}^2}\right)} \\ &\exp\left(\frac{-2r^2}{w_{\mathrm{L0}}^2}\right)r\,\mathrm{d}r = L + T_{\mathrm{oc}}\,.\end{aligned} \tag{23}$$

Let $x = \frac{2r^2}{w_{\mathrm{L0}}^2}$, $a = \frac{w_{\mathrm{L0}}^2}{w_{\mathrm{p0}}^2}$ and $y = \exp(-x)$, then (23) becomes

$$2\sigma\int_0^1 \frac{\tau\,(N_{\mathrm{tot}})\,\frac{2P_0\eta_{\mathrm{a}}}{h\nu_{\mathrm{p}}\pi w_{\mathrm{p0}}^2}y^a - f_{\mathrm{low}}N_{\mathrm{tot}}l}{1+\frac{4P_{\mathrm{c}}\tau(N_{\mathrm{tot}})\sigma}{h\nu_{\mathrm{L}}\pi w_{\mathrm{L0}}^2}y}\,\mathrm{d}y = L + T_{\mathrm{oc}}\,. \tag{24}$$

in (24), if $P_{\mathrm{c}} = 0$, the corresponding P_0 is the pump threshold P_{th}:

$$\begin{aligned}P_{\mathrm{th}} &= \frac{L + T_{\mathrm{oc}} + 2\sigma f_{\mathrm{low}}N_{\mathrm{tot}}l}{\int_0^1 \tau(N_{\mathrm{tot}})\frac{4\eta_{\mathrm{a}}\sigma}{h\nu_{\mathrm{p}}\pi w_{\mathrm{p0}}^2}y^a\,\mathrm{d}y} \\ &= \frac{h\nu_{\mathrm{p}}\pi w_{\mathrm{p0}}^2(a+1)(L + T_{\mathrm{oc}} + 2\sigma f_{\mathrm{low}}N_{\mathrm{tot}}l)}{4\eta_{\mathrm{a}}\tau(N_{\mathrm{tot}})\sigma}\,.\end{aligned} \tag{25}$$

3 Theoretical calculations comparing with experimental data

For quasi-four-level laser system such as Yb:YAG crystals, the pump power threshold of microchip laser expressed by (25) is strongly dependent on the optical properties of the gain medium (especially thermal loading parameter, the emission cross-section and fluorescence lifetime), the

pump condition (pump beam diameter), the intracavity loss, useful output coupling loss and the reabsorption loss at lasing wavelengths. The reabsorption loss is proportional to the Yb^{3+}-ion concentrations, thickness of the gain medium, and temperature-dependent thermal population distribution factor f_{low} at terminated laser levels of Yb:YAG crystal. Figure 2 shows the calculated absorbed pump power thresholds for 1030 nm and 1049 nm oscillation as a function of the transmission of the output coupler for different Yb concentrations. Both the absorbed pump power thresholds at 1030 nm and 1049 nm increase with T_{oc} for different Yb concentrations and the thickness of the Yb:YAG crystals. However, the absorbed pump power threshold at 1049 nm increases faster than that at 1030 nm with T_{oc}. There are transmissions of the output coupler ($T_{oc,dual}$) for dual-wavelength oscillation (4.8, 5.3 and 6.6% for 1-mm-thick Yb:YAG doped with 10, 15 and 20 at. % Yb^{3+}, respectively; 8.6% for 0.5-mm-thick Yb:YAG doped with 20 at. % Yb^{3+}). When these output couplings are used, the absorbed pump power thresholds at 1030 and 1049 nm are equal for different concentrations and thickness of Yb:YAG crystals. Therefore, dual-wavelength oscillation at 1030 nm and 1049 nm is possible by adjusting output coupling in microchip Yb:YAG lasers without controlling the loss by external factors, such as using different transmission of the output coupler. When T_{oc} is lower than $T_{oc,dual}$, the absorbed pump power threshold at 1049 nm is lower than that at 1030 nm; therefore, the laser prefers to oscillate at 1049 nm. Conversely, when T_{oc} is higher than $T_{oc,dual}$, the absorbed pump power threshold at 1030 nm is lower than that at 1049 nm; therefore, the laser prefers to oscillate at 1030 nm. Also the heat generated in the Yb:YAG gain medium plays a role on the laser oscillating wavelengths, as shown in Fig. 2. For a 1-mm-thick 10 at. % Yb:YAG microchip laser with $T_{oc} = 5\%$, the pump power threshold at 1030 nm is lower than that at 1049 nm; therefore, the laser oscillates at 1030 nm. The crystal temperature increases with a further increase of the pump power; therefore, the reabsorption loss increases, the value of the transmission of the output coupler for both wavelengths oscillation increases. Also, the threshold at 1049 nm is lower than that at 1030 nm, and the laser oscillates at 1049 nm for 10 at. % Yb:YAG, which is in fair agreement with the experimental observations of laser emitting wavelength switching from 1030 nm to 1049 nm for 10 at. % Yb:YAG microchip laser with $T_{oc} = 5\%$ [14]. For high Yb doping concentrations, owing to the strong reabsorption, the $T_{oc,dual}$ value for both wavelength oscillations are large; therefore, for $T_{oc} = 5\%$, the absorbed pump power threshold at 1049 nm is lower than that at 1030 nm, the lasers prefer to oscillate at 1049 nm. For $T_{oc} \geq 10\%$, the useful output coupling loss is large, the absorbed pump power threshold at 1049 nm is larger than that at 1030 nm, owing to the smaller emission cross-section at 1049 nm compared to that at 1030 nm. Therefore, the laser oscillates at 1030 nm. The cause of the change of laser wavelength and dual-wavelength operation for a 10 at. % Yb:YAG microchip laser with T_{oc} = 5% is attributed to the quasi-four-level nature of Yb:YAG and the local temperature rise due to the heat generated at high pump power. The local temperature rise inside Yb:YAG has a great effect on the thermal population distribution of terminated laser level for 1030 nm. Therefore the reabsorption around the strong emission peak of 1030 nm increases, the threshold for 1030 nm oscillation increases; however, the local temperature rise has little effect on the reabsorption loss around the weak emission peak of 1049 nm for Yb:YAG crystal, there is a tradeoff between 1030 and 1049 nm lasing. With a further increase of the local temperature, the laser prefers to oscillate at 1049 nm rather than at 1030 nm with $T_{oc} = 5\%$. Therefore, when the absorbed pump power is higher than a certain value, the laser oscillates at 1049 nm. For heavy-doped Yb:YAG crystals (15 and 20 at. %), the reabsorption loss plays an important role in the laser oscillation threshold, the laser prefers to oscillate at 1030 nm that at 1049 nm.

The numerical simulations of Yb:YAG microchip lasers [14] were performed by taking into account the reabsorption loss relating to the local temperature rise due to heat generation inside the gain crystal by absorbed pump power, temperature-dependent stimulated emission cross-section, thermal conductivity [8], concentration-dependent fluorescence lifetime, thermal loading [8] and so on. The parameters of the laser cavity and the Yb:YAG laser material used in the numerical simulations are listed in Table 1. The stimulated

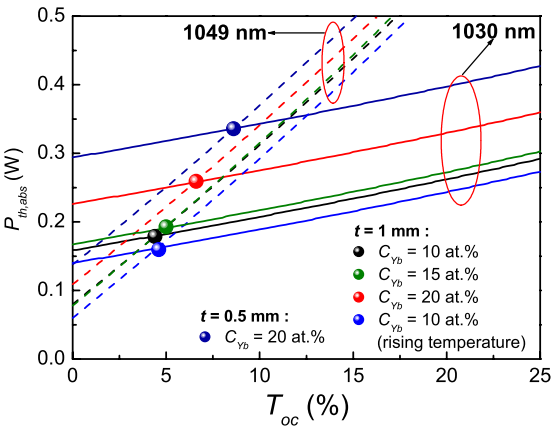

FIGURE 2 The absorbed pump power thresholds at 1030 nm and 1049 nm as a function of transmission of the output coupler for Yb:YAG crystals doped with different Yb^{3+} lasants. The effect of temperature rise on the pump power thresholds for 10 at. % Yb:YAG at both wavelengths are also shown

Parameters	Value
λ_p	940 nm
λ	1030 nm
	1049 nm
w_{p0}	60 μm
w_{L0}	60 μm
P_0	10.5 W
T_0	0.05, 0.1, 0.15 and 0.2
δ	0.002 cm^{-1} for 10 at. % Yb
	0.004 cm^{-1} for 15 at. % Yb
	0.006 cm^{-1} for 20 at. % Yb
l	1 mm
	0.5 mm
C_0	39 at. %
n	1.82
C_r	0.0195
ν	0.3

TABLE 1 Parameters for Yb:YAG microchip lasers used in the theoretical simulations

emission cross-section, σ, and the thermal population fraction f_{low} and f_{up} of Yb:YAG crystal are strongly dependent on the temperature [21]. The relationship between the stimulated emission cross-section of Yb:YAG crystal and temperature can be described as

$$\sigma(T) = 2 + \frac{10.5}{1+\exp\left(\frac{T-131.6}{52}\right)} \times 10^{-20}\,\mathrm{cm}^2 \quad [21]\,.$$

Concentration-dependent fluorescence lifetime, $\tau(N_{\mathrm{tot}})$, can be described as $\tau(N_{\mathrm{tot}}) = (0.67442 + 0.37632\exp(-C/C_0)) \times 10^{-3}$ s [21], where C is the atomic percentage of the doping ions, C_0 is the parameter that describes the concentration quenching effect in Yb:YAG crystal. The laser performance was simulated by numerically solving the (24) for YAG crystals doped with different Yb^{3+}-ion concentrations under different output coupling conditions. The numerical simulations of the output power for microchip lasers with different Yb^{3+}-ion concentrations as a function of the incident pump power under different coupling conditions for 1049 nm ($T_{\mathrm{oc}} = 5\%$) and 1030 nm ($T_{\mathrm{oc}} = 10\%$) oscillations are shown in Fig. 3 together with the experimental data taken from [14]. The numerical simulations of the laser performance (output power, optical-to-optical efficiency with respect to the incident pump power are listed in Table 2) are in good agreement with the experimental data for different working conditions. The numerical simulation results show that 1-mm-thick Yb:YAG crystals doped with different concentration ($C_{\mathrm{Yb}} = 10$, 15 and 20 at. %) laser operation at 1049 nm can be used for achieving comparable laser output, and the laser performance is little better for higher concentration. However, the laser performance of 0.5-mm-thick Yb:YAG ($C_{\mathrm{Yb}} = 20$ at. %) is not improved compared to 1-mm-thick Yb:YAG ($C_{\mathrm{Yb}} = 20$ at. %) with respect to the incident pump power. For 1030 nm laser oscillation, the output power decreases with Yb concentration for 1-mm-thick Yb:YAG microchip lasers owing to the strong reabsorption at the terminated laser level. The best laser performance at 1030 nm was achieved by using Yb:YAG ($C_{\mathrm{Yb}} = 10$ at. %) with smaller reabsorption loss. The thin Yb:YAG ($C_{\mathrm{Yb}} = 20$ at. %) does not benefit the laser performance at 1030 nm, and even worse than that working at 1049 nm. It should be noted that (24) does not take into account of the thermal lens effect induced by the heat generation resulted from absorbed pump power; therefore, the output power increases with pump power even when the pump power exceeds the critical pump power limited by the thermal lens and thermal deformation effects, making the laser resonator unstable and causing the laser to stop.

Figure 4 shows the output power as a function of the thickness of Yb:YAG crystal doped with different Yb concentrations. The incident pump power was set to 10.5 W in the simulations. Laser output power at 1049 nm oscillation with $T_{\mathrm{oc}} = 5\%$ is higher than that at 1030 nm oscillation with $T_{\mathrm{oc}} = 10\%$ for all the Yb concentrations ($C_{\mathrm{Yb}} = 10$, 15, and 20 at. %). Optimized thickness of Yb:YAG crystal is different for 1049 nm and 1030 nm oscillation, the optimized thick-

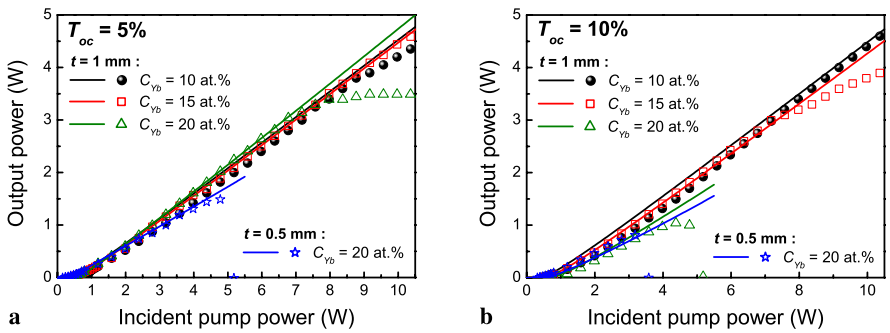

FIGURE 3 The numerical simulations of the output power of Yb:YAG microchip lasers under different working conditions for (**a**) 1049 nm and (**b**) 1030 nm oscillations. The *dots* are the experimental data taken from [14]

Yb:YAG	T_{oc} (%)	λ_{L} (nm)	P_{in} (W)	P_{out} (W)		$\eta_{\mathrm{o-o(in)}}$ (%)	
				Exp.	Cal.	Exp.	Cal.
10 at. %, 1 mm thick	5	1049	10.5	4.35	4.77	43	45
	10	1030	10.5	4.6	4.73	44	45
	15	1030	10.5	3.5	4.19	34	40
	20	1030	10.5	3.4	3.74	33	40
15 at. %, 1 mm thick	5	1049	10.5	4.6	4.73	44	45
	10	1030	10.5	3.9	4.51	41	43
	15	1030	10.5	3.5	4.24	36	40
	20	1030	10.5	3.3	3.96	36	38
20 at. %, 1 mm thick	5	1049	10.5	3.05	5.01	45	48
	10	1030	5.5	1.04	1.77	24	32
	15	1030	5	0.9	1.45	21	29
	20	1030	5	0.71	1.27	18	25
20 at. %, 0.5 mm thick	5	1049	5.5	1.5	1.93	33	35
	10	1030	5.5	0.81	1.56	26	28
	15	1030	5	0.48	1.3	17	26
	20	1030	3.5	0.38	0.67	14	19

TABLE 2 Comparison of calculated and experimental results for microchip Yb:YAG lasers. Experimental data of output power and optical-to-optical efficiency are the maximum values obtained from experiments. P_{in} is the value used in numerical calculations, which is close to the experimental conditions

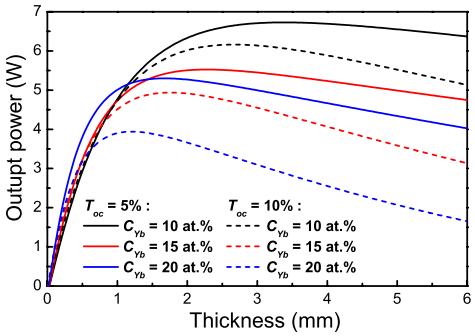

FIGURE 4 Output power of Yb:YAG microchip lasers as a function of the thickness of Yb:YAG crystals for different Yb concentrations. The incident pump power was set to 10.5 W when the calculations were performed

ness of Yb:YAG crystal at 1049 nm oscillation is thicker than that at 1030 nm. The better laser performance can be obtained by choosing thicker Yb:YAG doped with lower Yb concentrations or thin Yb:YAG crystal with high Yb concentration. Optimized crystal lengths working at 1049 nm are 3.38, 2.28 and 1.7 mm for Yb:YAG crystal doped with 10, 15 and 20 at. % Yb^{3+}-lasant. Therefore, the optical-to-optical efficiency of over 59% at 1049 nm with respect to the incident pump power can be achieved by using 10 at. % Yb:YAG with optimized thickness of 3.38 mm and $T_{oc} = 5\%$. Optimized crystal length (2.67, 1.75 and 1.2 mm for Yb:YAG crystal doped with 10, 15 and 20 at. % Yb^{3+}-lasant) is shortened for 1030 nm operation owing to strong thermal population distribution compared to that at 1049 nm. For 1-mm-thick Yb:YAG crystals, laser performance at 1049 nm of 20 at. % Yb:YAG with respect to the incident pump power is better than that of 10 and 15 at. % because the thickness of Yb:YAG crystal is close the optimized thickness. Laser performance becomes worse by using thinner crystal (< 1 mm) for single-pass end-pumped Yb:YAG microchip lasers. Figure 5 shows the output power of 1-mm-thick Yb:YAG microchip lasers at 1049 nm and 1030 nm as a function of the transmission of the output coupler for different Yb concentrations under 10.5 W incident pump power. For 1049 nm oscillation, output power for 20 at. % Yb:YAG with $T_{oc} = 5\%$ is better than those for 10 and 15 at. % Yb:YAG, which is in good agreement with the experimental data without considering the strong thermal lens effect in highly doped Yb:YAG microchip lasers.

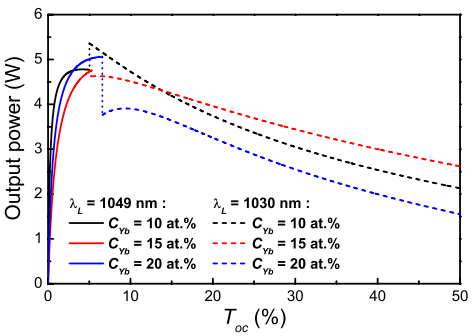

FIGURE 5 Output power of Yb:YAG microchip lasers as a function of the transmission of the output coupler for different Yb doping concentrations. The incident pump power was set to 10.5 W when the calculations were performed

However, for 1030 nm operation, the effect of output coupling on 10 at. % Yb:YAG microchip laser is stronger than on 15 and 20 at. % Yb:YAG microchip lasers. The output power of 10 at. % Yb:YAG microchip laser decreases faster with T_{oc} than those for 15 and 20 at. % Yb:YAG microchip lasers when $T_{oc} > 10\%$. For $T_{oc} = 10\%$, the output power of 10 at. % Yb:YAG microchip laser is higher than those from 15 and 20 at. % Yb:YAG, however, with further increase of T_{oc}, the output power of 15 at. % is higher than those from 10 and 20 at. % Yb:YAG when $T_{oc} > 14\%$. Under certain output coupling, the optimizing laser performance of end-pumped Yb:YAG microchip lasers can be achieved by adopting thick Yb:YAG crystals doped with low Yb concentration. With current available fiber-coupled laser-diode as pump source, the large Rayleigh range (several millimeters depending on the pump beam diameter incident on the laser crystal) from laser-diode can be obtained, for optimized 3.38-mm-thick Yb:YAG doped with 10 at. % Yb ions can be well pumped and relative uniform pump power distribution can be achieved.

Although numerical simulations of microchip laser performance of Yb:YAG crystals doped with different Yb concentrations are in good agreement with experimental data (as shown in Fig. 3), the output power roll-over observed in the experiments cannot be fully explained by the thermal population distribution inside the gain medium and reabsorption loss, because the average temperature rise along the thickness of gain medium is assumed for the simplified calculations. However, for end-pumped Yb:YAG microchip laser, owing to the absorbed pump power distribution as an exponential decay along the thickness of gain medium; therefore, the temperature distribution inside its gain crystal is different along the thickness and the radius of the generated crystal. Figure 6 shows the temperature distribution along the thickness and the radius of YAG crystals doped with different Yb^{3+}-ion concentration according to (5), the incident pump power of 10.5 W for 10 and 15 at. % Yb:YAG and 5 W for 20 at. % Yb:YAG was used in the calculation of the temperature distribution. The maximum temperature rise locates at the entrance

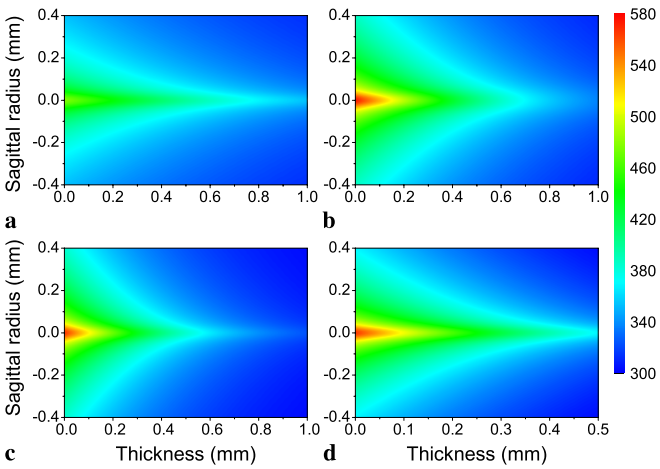

FIGURE 6 Temperature profile distribution along the thickness and radius of Yb:YAG crystals for (**a**) 10 at. % Yb:YAG under 10.5 W incident pumping; (**b**) 15 at. % Yb:YAG under 10.5 W incident pumping; (**c**) 20 at. % Yb:YAG under 5 W incident pumping; (**d**) 0.5-mm-thick Yb:YAG doped with 20 at. % Yb under 5 W incident pumping

of the pump beam incident on the Yb:YAG crystal, the temperature decreases along the thickness because the absorbed pump power decreases exponentially. Temperature increases with Yb^{3+}-ion concentration under the same pump power level (as shown in Fig. 6a and b). The temperature for 20 at. % Yb:YAG crystal (Fig. 6c and d) even with only 5 W incident pump power is close to that for 15 at. % Yb:YAG crystal (Fig. 6b) under 10.5 W incident pump power. For heavy-doped Yb:YAG crystals, the temperature difference between the entrance surface and the exit surface is larger than that for low doped Yb:YAG crystals. Temperature of working Yb:YAG crystal increases with absorbed pump power, and the temperature is higher for heavy-doped Yb:YAG crystals than that for low doping Yb:YAG crystals under the same pump power levels. Therefore, the thermally induced population distribution at the terminated laser levels is large for heavy-doped Yb:YAG crystals and makes the laser performance less efficient.

The temperature rise in Yb:YAG gain medium induced by the absorbed pump power inside the gain medium leads to strong thermally induced lenses and decreases in the critical pump power for stable laser oscillation according to (7) and (10). Because the thermal conductivity becomes worse for YAG doped with heavy concentration of Yb^{3+}-ion, the thermal loading coefficient is getting larger for heavy-doped Yb:YAG crystal [8]; therefore, the critical pump power range for stable laser oscillation is narrower for heavy-doped crystals. The critical pump powers were calculated to be 49, 31, and 10.4 W for 1-mm-thick 10, 15, and 20 at. % Yb:YAG crystals. The laser performance of heavy-doped Yb:YAG microchip lasers is limited by the thermal lens effect: the higher the concentration, the stronger the thermal lens effect, the narrower the critical pump power range. Although the critical pump power becomes smaller with Yb concentration, the calculated critical pump power for YAG crystals doped with different ytterbium concentrations is still higher than that in the experiments using heavy-doped Yb:YAG crystals. This was caused by the uncertainty of the thermal properties of heavy-doped Yb:YAG crystals. The thermal lens effects induced by the absorbed pump power in the gain medium have great effect on the laser output beam, whose diameter becomes smaller with enhanced thermal lens effect for heavy-doped Yb:YAG crystals, which is one of the causes for the roll-over of the output power for Yb:YAG microchip lasers observed in the laser experiments. According to (10), the critical pump power is inversely proportional to the thickness of the gain medium; therefore, the critical pump power for 0.5-mm-thick Yb:YAG was calculated to be 22 W for 0.5-mm-thick Yb:YAG crystal doped with 20 at. % Yb and was larger than that for 1-mm-thick Yb:YAG; however, these results contradict the experimental results of 20 at. % Yb:YAG with different thicknesses (as shown in Fig. 3). The difference between the experimental data and theoretical calculations of critical pump power for 20 at. % Yb:YAG crystal with different thicknesses is caused by the fact that we did not take into account the thermal deformation of thin crystal under high pump power. The thermal deformation in thin crystal is severer than that in thick crystal and is another main reason for the small critical pump power for thin gain medium. The combination effects of thermal lens and thermal deformation in thin crystal result in a decrease of the output power or even cause the output laser to stop.

Besides the thermal lens effect and thermal deformation effect limiting, the laser performance in a single-pass end-pumped Yb:YAG microchip laser, the saturated inversion population distribution also has a great effect on the laser performance. Equation (20) expresses the spatial distribution of the saturated inversion population density along the thickness and radius of Yb:YAG crystal including the reabsorption loss due to the thermal distribution in terminated laser levels. By taking into account the temperature effect, we show the saturated inversion population distribution inside Yb:YAG crystals with 10 and 15 at. % Yb^{3+}-ion concentrations at two terminated laser levels under 10.5 W incident pump power in Fig. 7. The inversion population distribution along the thickness of Yb:YAG crystal with high doping concentration has larger variation between the entrance surface and exit surface of the pump power beam. Therefore, for heavy-doped Yb:YAG crystal, the entrance section is well pumped, but the inversion population close to the exit section may be not useful for the laser oscillation, owing to the lower inversion population. The gain at the exit section cannot overcome the resonator losses including the reabsorption loss, the reabsorption loss becomes severe with heavy-doped Yb:YAG crystal. In particular, this effect is stronger at 1030 nm oscillation that that at 1049 nm, because of the strong reabsorption loss at 1030 nm compared to that at 1049 nm for Yb:YAG crystal. The effective gain length is shorter than the Yb:YAG crystal length, a poor pump section acts as an additional loss to the laser oscillation. Therefore, the performance of heavy-doped Yb:YAG microchip lasers become worse compared to the lower Yb^{3+}-ion concentration YAG crystal (as indicated in Fig. 2 in [14]). Figure 8 shows the saturated inversion population inside 1-mm-thick and 0.5-mm-thick YAG crystal with 20 at. % Yb^{3+} dopants at 1.05 and 1.03 μm oscillations under 5 W incident pump power. By shortening the Yb:YAG thickness, although the temperature distribution along the thickness and radius is the same for different thick-

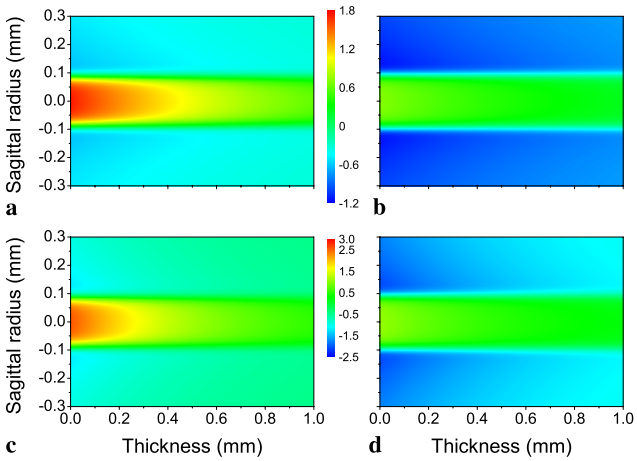

FIGURE 7 Saturated inversion population distribution along the thickness and sagittal radius of 1-mm-thick Yb:YAG microchip lasers under 10.5 W incident pump power, at (**a**) 1.05 μm and (**b**) 1.03 μm oscillation for 10 at. % Yb:YAG; at (**c**) 1.05 μm and (**d**) 1.03 μm oscillation for 15 at. % Yb:YAG. The unit of the saturated inversion population is $\times 10^{20}$ cm^{-3}

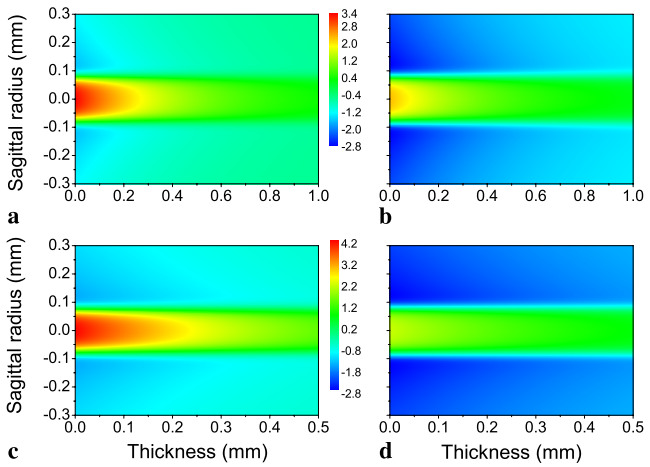

FIGURE 8 Saturated inversion population distribution along the thickness and sagittal radius of 20 at. % Yb:YAG microchip lasers under 5 W incident pump power, at (**a**) 1.05 μm and (**b**) 1.03 μm oscillation for 1-mm-thick Yb:YAG; (**c**) 1.05 μm and (**d**) 1.03 μm oscillation for 0.5-mm-thick Yb:YAG. The unit of the saturated inversion population is $\times 10^{20}$ cm^{-3}

nesses of Yb:YAG crystals doped with 20 at. % Yb^{3+}-ions, the average temperature rise inside the thin gain medium is higher than that in thick gain medium because the temperature is inversely proportional to the thickness of gain crystal for such microchip lasers, the thinner the gain medium, the higher the temperature as indicated in (6). Therefore, the laser performance is worse than the thick crystal with 20 at. % Yb^{3+} dopants. The saturated inversion population distribution inside the gain medium is another important factor affecting the laser performance of heavy-doped Yb:YAG microchip lasers. As discussed above, the output power roll-over of Yb:YAG microchip lasers at room temperature without actively cooling the gain medium is caused by the combined effect of the thermal lens effect, thermal deformation and saturated inversion population distribution inside the gain medium. For Yb:YAG doped with low Yb concentration, the thermal properties are better than those of Yb:YAG doped with high Yb concentration; thick crystal is favorable for laser performance. However, for high concentration Yb:YAG crystals, although thin crystal can increase the critical pump power, Yb:YAG with thin crystal length is more easily deformed by the heat generated inside the gain medium. Therefore, the laser cavity becomes unstable with thin crystals and high doping concentration, causing the laser to stop. Here, the thermal deformation of the thin gain medium is the dominant factor for determining the critical pump power other than the thermal lens effect in the case of heavy-doped Yb:YAG crystals.

4 Conclusions

In conclusion, the performance of Yb:YAG microchip lasers is simulated based on the rate equations, including the reabsorption loss and temperature-dependent emission peak cross-section and concentration-dependent thermal properties and luminescence lifetime of the $^2F_{5/2}$ state. The calculated results are in good agreement with the experimental data. Besides the effect of thermal population distribution and other temperature- and Yb concentration-dependent parameters, we also discussed the thermal lens effect, thermal deformation effect, and saturated inversion population distribution inside the gain medium, which are also important factors for limiting the laser performance of Yb:YAG microchip lasers, especially for heavy-doped Yb:YAG microchip lasers working at 1030 nm. The oscillating wavelength was analyzed by comparing the absorbed pump power threshold at different laser wavelengths for different output coupling and Yb concentrations. Wavelength switching from 1030 nm to dual-wavelength oscillation and then 1049 nm oscillation was explained by the absorbed pump power thresholds at 1030 nm and 1049 nm for 10 at. % Yb:YAG microchip laser with $T_{oc} = 5\%$. The performance of Yb:YAG microchip laser at 1049 nm is better than that at 1030 nm owing to the weak reabsorption loss. The laser performance of Yb:YAG microchip lasers can be further improved by choosing optimized crystal thickness at room temperature, the optical-to-optical efficiency of over 59% at 1049 nm with respect to the incident pump power can be achieved by using 10 at. % Yb:YAG with optimized thickness of 3.38 mm.

ACKNOWLEDGEMENTS This work was supported by the 21st Century Center of Excellence (COE) program of Ministry of Education, Science, Sports, and Culture of Japan. One of us (A.A.K.) wishes to acknowledge the Russian Foundation for Basic Research.

REFERENCES

1 A. Giesen, H. Hugel, A. Voss, K. Wittig, U. Brauch, H. Opower, Appl. Phys. B **58**, 365 (1994)
2 T.S. Rutherford, W.M. Tulloch, E.K. Gustafson, R.L. Byer, IEEE J. Quantum Electron. **QE-36**, 205 (2000)
3 A.A. Kaminskii, *Laser Crystals* (Springer, Berlin, Heidelberg, New York, 1981)
4 D.S. Sumida, T.Y. Fan, Opt. Lett. **19**, 1343 (1994)
5 G.A. Bogomolova, D.N. Vylegzhanin, A.A. Kaminskii, Sov. Phys. JETP **42**, 440 (1976)
6 T.Y. Fan, IEEE J. Quantum Electron. **QE-29**, 1457 (1993)
7 H.W. Bruesselbach, D.S. Sumida, R.A. Reeder, R.W. Byren, IEEE J. Sel. Top. Quantum Electron. **3**, 105 (1997)
8 F.D. Patel, E.C. Honea, J. Speth, S.A. Payne, R. Hutcheson, R. Equall, IEEE J. Quantum Electron. **QE-37**, 135 (2001)
9 E.C. Honea, R.J. Beach, S.C. Mitchell, J.A. Sidmore, M.A. Emanuel, S.B. Sutton, S.A. Payne, P.V. Avizonis, R.S. Monroe, D. Harris, Opt. Lett. **25**, 805 (2000)
10 C. Stewen, K. Contag, M. Larionov, A. Giessen, H. Hugel, IEEE J. Sel. Top. Quantum Electron. **6**, 650 (2000)
11 M. Tsunekane, T. Taira, Opt. Lett. **31**, 2003 (2006)
12 Q. Liu, M. Gong, F. Lu, W. Gong, C. Li, D. Ma, Appl. Phys. Lett. **88**, 101 113 (2006)
13 H. Bruesselbach, D.S. Sumida, IEEE J. Sel. Top. Quantum Electron. **11**, 600 (2005)
14 J. Dong, A. Shirakawa, K. Ueda, A.A. Kaminskii, Appl. Phys. B **89** (2007), DOI: 10.1007/s00340-007-2796-2
15 T.Y. Fan, R.L. Byer, IEEE J. Quantum Electron. **QE-23**, 605 (1987)
16 W.P. Risk, J. Opt. Soc. Am. B **5**, 1412 (1988)
17 G.L. Bourdet, G. Lescroart, Opt. Commun. **149**, 404 (1998)
18 A.J. Alfrey, IEEE J. Quantum Electron. **QE-25**, 760 (1989)
19 Z. Huang, Y. Huang, M. Huang, Z. Lou, J. Opt. Soc. Am. B **20**, 2061 (2003)
20 T. Taira, J. Saikawa, T. Kobayashi, R.L. Byer, IEEE J. Sel. Top. Quantum Electron. **3**, 100 (1997)
21 J. Dong, M. Bass, Y. Mao, P. Deng, F. Gan, J. Opt. Soc. Am. B **20**, 1975 (2003)
22 D.S. Sumida, T.Y. Fan, in *Advanced Solid-State Lasers*, ed. by T.Y. Fan, B.H.T. Chai (Optical Society of America, Washington, DC, 1994) Vol. 20, p. 100
23 W. Kochner, *Solid State Laser Engineering* (Springer, Berlin, 1999)
24 M.E. Innocenzi, H.T. Yura, C.L. Fincher, R.A. Fields, Appl. Phys. Lett. **56**, 1831 (1990)

25 D. Metcalf, P. De-Giovanni, J. Zachorowski, M. Leduc, Appl. Opt. **26**, 4508 (1987)
26 A.K. Cousins, IEEE J. Quantum Electron. **QE-28**, 1057 (1992)
27 H. Kogelnik, T. Li, Proc. IEEE **54**, 1312 (1966)
28 R. Ifflander, H.P. Kortz, H. Weber, Opt. Commun. **29**, 223 (1979)
29 G.A. Slack, D.W. Oliver, Phys. Rev. B **4**, 592 (1971)
30 T.Y. Fan, J.L. Daneu, Appl. Opt. **37**, 1635 (1998)
31 R. Wynne, J.L. Daneu, T.Y. Fan, Appl. Opt. **38**, 3282 (1999)
32 D.C. Brown, IEEE J. Quantum Electron. **QE-33**, 861 (1997)
33 T.Y. Fan, R.L. Byer, IEEE J. Quantum Electron. **QE-24**, 895 (1988)